JOURNAL OF THERMOPHYSICS AND HEAT TRANSFER
Vol. 10, No. 3, July–September 1996

Direct Simulation of Shock Front Radiation in Air

A. K. Berghausen*
North Carolina State University, Raleigh, North Carolina 27695-7910
J. C. Taylor†
Johns Hopkins University, Applied Physics Laboratory, Laurel, Maryland 20723-6099
and
H. A. Hassan‡
North Carolina State University, Raleigh, North Carolina 27695-7910

An absorption model has been incorporated in a simulation of shock front radiation in air at a shock velocity of 10.2 km/s and a pressure of 0.1 torr. The conditions selected correspond to two shock-tube experiments carried out at AVCO and NASA Ames Research Center. Comparisons are made with experiment, with another absorption model, and with recent continuum calculations. In general, calculated intensities are within a factor of 2–4 of measured values. Moreover, allowing for absorption brought prediction of the intensity of $N_2^+(1-)$ well within experimental error.

Nomenclature

A = transition probability
B = particle in electronically excited state
c = speed of light
g = degeneracy of an electronic state
h = Planck constant
K = excitation rate coefficient
k = Boltzmann constant
M = arbitrary collision partner
N = total number of particles
R_f = random fraction between 0 and 1
S = absorption distance for photons
S^* = random portion of length ΔS
T = collision temperature
ΔS = distance from emitter to boundary
ε = energy of an electronic state
κ_υ = volumetric absorption coefficient
κ_υ^* = value of κ_υ corresponding to S^*
λ = wavelength of emission
τ = mean lifetime
υ = frequency, c/λ
$\bar{\upsilon}$ = collision frequency
ϕ = fraction of energy radiated from electronic level

Subscripts
i = electronic state
j = lower of two electronic states
k = upper of two electronic states

Superscripts
f = final conditions
i = initial conditions

Presented as Paper 95-2051 at the AIAA 30th Thermophysics Conference, San Diego, CA, June 19–22, 1995; received July 21, 1995; revision received Jan. 15, 1996; accepted for publication March 21, 1996.

*Graduate Research Assistant, Department of Mechanical and Aerospace Engineering. e-mail: akbergha@jupiter1.mae.ncsu.edu. Member AIAA.
†Postdoctoral Fellow. Member AIAA.
‡Professor, Department of Mechanical and Aerospace Engineering. Associate Fellow AIAA.

Introduction

THE direct simulation Monte Carlo (DSMC) method of Bird[1] has emerged as a highly reliable computational tool for calculating hypersonic flows over re-entry vehicles. Such hypersonic flows are characterized by high degrees of thermal, chemical, and radiative nonequilibrium. At re-entry velocities of interest, nonequilibrium radiation can contribute a significant portion of the heat load. Therefore, it is imperative that adequate computational tools be developed to estimate the contribution of this important mode of heat transfer.

The ability of DSMC to model nonequilibrium radiation was demonstrated in Refs. 2–5. In these calculations, radiation was assumed to be optically thin. More recently, Taylor et al.[6] introduced an absorption model in the study of the Fire II vehicle. They demonstrated the importance of absorption in bringing the predictions of theory well within accepted scatter of the experiment.

Attempts at a DSMC simulation of the AVCO experiment,[7] in which measurements were carried out in an electric arc-driven shock tube on a normal shock wave in air at 10 km/s and 0.1 torr, were undertaken by Bird[2] and Carlson and Hassan[4] using a stagnation streamline calculation.[1] The need to use such an approach results from the consideration that normal shock codes require specification of the equilibrium conditions downstream. Because of the slow recombination rates in rarefied flows, however, equilibrium conditions can only be achieved at a large distance from the shock center, thus rendering such computations impractical. Except for the overpredictions of the intensity of the $N_2^+(1-)$ system, Ref. 4 obtained good qualitative agreement with the AVCO experiment. The relaxation numbers employed, ratios of collision to excitation cross sections, were obtained from rates developed in the nonequilibrium air radiation (NEQAIR) program.[8]

Since the completion of the work in Ref. 4, new experimental data, computational results, and DSMC techniques have become available. Sharma et al.[9] have repeated the AVCO experiment at NASA Ames. These new data were compared with continuum radiation calculations carried out by Sharma and Whiting.[10] The results of the comparisons were mixed: good agreement of the intensity of the $N_2^+(1-)$ system, overpredictions of intensities of the various O and N atomic transitions, and underprediction of the intensities of the $N_2(2+)$ system. On the simulation side, improved relaxation numbers and an absorption model suited for DSMC calculations have also been developed in Ref. 6.

The objective of this work is to simulate the Ames experiment using the latest enhancements of DSMC and a new implementation of the absorption model of Ref. 6.

Approach

Computational Domain and Procedure

The computational domain consisted of a region 3.5 cm in length divided into 520 computational cells distributed among four distinct regions. All cell sizes met the computational requirements of DSMC, i.e., all cell sizes were within one-third of a local mean free path. Approximately 220,000 particles were used.

The stagnation streamline code employed is based on that given in Ref. 1 together with the modifications employed in Refs. 4, 6, and 11. Eleven species and 41 chemical reactions were considered.[2,4] Only bound–bound radiative transitions, 26 in all, were permitted and are listed in Table 1.

Because of the large number of radiative states and because a significant fraction of radiation comes from sparsely populated states and minor species, each excited particle is assigned a distribution over all available states. The list of all states considered is given in Tables 2 and 3. As seen from the tables, grouping of the various states has been performed to keep the number of levels somewhat manageable. As a consequence of this grouping, each transition generally involves a fraction ϕ of the states in the upper group,[2,4] listed in Table 1.

The sampled electronic energy can be written as an average of the electronic states, i.e.,

$$\langle \varepsilon_{el} \rangle = \left(\sum \varepsilon_i N_i \right) \Big/ N \tag{1}$$

with

$$\frac{N_i}{N} = \frac{g_i \exp[-\varepsilon_i/(kT)]}{\sum g_i \exp[-\varepsilon_i/(kT)]} \tag{2}$$

The sum is taken over all energies of electronic states given in Tables 2 and 3. Equation (2) assumes that the distribution of states of a particular particle is a Boltzmann distribution at the temperature determined from the relative energy of the specific collision that produces the excitation.

For bound–bound transitions, the dominant excitation reactions can be written as

$$M + B_j \leftrightarrow M + B_k \tag{3}$$

$$B_k \leftrightarrow B_j + h\nu \tag{4}$$

It is shown in Ref. 4 that the electronic collision numbers are given by $\tau\bar{\nu}$, where $\bar{\nu}$ is the collision frequency and τ is given by

$$\frac{1}{\tau} = \frac{\sum \varepsilon_j N_j [K_M(j) N_M + A(j)]}{\sum \varepsilon_j N_j} \tag{5}$$

with

$$K_M(j) = \sum_k K_M(j, k) \tag{6}$$

$$A(j) = \sum_k A(j, k) \tag{7}$$

The previous relaxation numbers are required for partitioning of electron energy when a Borgnakke–Larsen[12] approach is implemented.

Table 1 Radiative mechanisms used in simulation

Molecule/ band	Transition	τ, s	λ, μ	ϕ
N_2,1+	3 → 2	1.1×10^{-5}	1.06	1.0
N_2,2+	5 → 3	2.7×10^{-8}	0.34	1.0
O_2,S-R	5 → 1	8.2×10^{-9}	0.20	1.0
NO,β	3 → 1	6.7×10^{-7}	0.22	1.0
NO,γ	2 → 1	1.16×10^{-7}	0.23	1.0
N_2^+,1−	3 → 1	6.7×10^{-8}	0.39	1.0
O	5 → 4	3.3×10^{-8}	0.83	0.6
	6 → 1	2.5×10^{-8}	0.103	0.1
	6 → 4	2.0×10^{-6}	0.45	0.01
	6 → 5	2.5×10^{-8}	0.99	0.7
	7 → 1	0.4×10^{-8}	0.099	0.1
	7 → 5	1.0×10^{-7}	0.64	0.4
	8 → 5	5.0×10^{-7}	0.55	0.1
N	4 → 1	0.5×10^{-8}	0.117	0.5
	4 → 2	0.2×10^{-8}	0.152	0.25
	4 → 3	0.5×10^{-8}	0.178	0.25
	5 → 2	0.2×10^{-8}	0.129	0.15
	5 → 4	6.0×10^{-8}	0.907	0.08
	6 → 2	1.0×10^{-8}	0.117	0.1
	6 → 3	1.0×10^{-8}	0.132	0.1
	6 → 5	5.0×10^{-8}	1.19	0.7
	7 → 4	1.0×10^{-6}	0.45	0.1
	8 → 2	3.0×10^{-8}	0.108	0.005
	8 → 3	5.0×10^{-8}	0.121	0.003
	8 → 4	2.5×10^{-7}	0.38	0.008
	8 → 5	1.0×10^{-7}	0.65	0.04

Table 2 Molecular electronic energy levels

Molecule	State	Energy, J	Degeneracy
O_2	$1(X^3\sigma)$	0	3
	$2(a^1\Delta)$	1.573×10^{-19}	2
	$3(b^1\sigma)$	2.621×10^{-19}	1
	$4(A^3\sigma)$	7.169×10^{-19}	3
	$4(B^3\sigma)$	9.891×10^{-19}	3
N_2	$1(X^1\sigma)$	0	1
	$2(a^3\sigma)$	9.971×10^{-19}	3
	$3(B^3\pi)$	1.184×10^{-18}	6
	$4(a^1\pi)$	1.376×10^{-18}	6
	$5(C^3\pi)$	1.771×10^{-18}	2
N_2^+	$1(X^2\sigma)$	0	2
	$2(A^2\pi)$	1.791×10^{-19}	2
	$3(B^2\sigma)$	5.077×10^{-19}	2
	$4(D^2\pi)$	1.026×10^{-18}	2
NO	$1(X^2\pi)$	0	4
	$2(a^2\sigma)$	8.732×10^{-19}	2
	$3(B^2\pi)$	9.122×10^{-19}	4
	$4(C, D^2\sigma)$	1.045×10^{-18}	4
	$5(E^2\sigma)$	1.204×10^{-18}	2

Table 3 Atomic electronic energy levels

Atom	Group	Energy, J	Degeneracy
O	1	0	9
	2	3.16×10^{-19}	5
	3	6.71×10^{-19}	1
	4	1.49×10^{-18}	8
	5	1.73×10^{-18}	24
	6	1.93×10^{-18}	72
	7	2.04×10^{-18}	128
	8	2.09×10^{-18}	848
N	1	0	4
	2	3.82×10^{-19}	10
	3	5.73×10^{-19}	6
	4	1.688×10^{-18}	18
	5	1.907×10^{-18}	54
	6	2.073×10^{-18}	108
	7	2.127×10^{-18}	54
	8	2.214×10^{-18}	1314

Absorption Model

The probability of a photon traveling a distance S before absorption occurs is determined from[13]

$$\exp\left(-\int_0^S \kappa_\nu \, dS\right) = R_f \tag{8}$$

The coefficient κ_ν is a function of number densities and temperatures and is readily available from existing radiation codes such as NEQAIR (Ref. 8) and LORAN (Ref. 14). Because the charged particles are a minority species, κ_ν was calculated over supercells, or collections of 10 adjacent computational cells, to achieve an adequate sample of charged particles.

Equation (8) can be solved iteratively for S. This, however, is an expensive procedure. As a result a simple procedure needs to be developed to calculate S. In the procedure of Ref. 6 a representative value of κ_ν, called κ_ν^*, is chosen based upon a random selection of an absorption coefficient between the cell in which emission occurred, denoted by i, and the last cell in the computational domain in the direction of emission, denoted by f, i.e.,

$$\kappa_\nu^* = \kappa_\nu^i + R_f(\kappa_\nu^f - \kappa_\nu^i) \tag{9}$$

Because the approximation for κ_ν^* given by Eq. (9) is based entirely upon information at two points, it will underpredict κ_ν^* for photons emitted through the shock because the values for κ_ν^i and κ_ν^f will be small on either side of the shock. The absorption coefficients within the shock, however, are quite large (Fig. 1).

To allow for the larger values of κ_ν within the shock a new method for efficiently determining κ_ν^* is utilized. The direction of a radiation event θ is chosen such that all directions are equally possible. If ΔS is the distance between the point of emission and the computational boundary measured along the direction of θ, then a representative κ_ν^* in Eq. (8) is that value corresponding to S^*, determined from

$$S^* = R_f \Delta S \tag{10}$$

This representative value of κ_ν^* is then used in Eq. (8) to determine the absorption distance, S, i.e.,

$$S = -\ell n(R_f)/\kappa_\nu^* \tag{11}$$

If $S > \Delta S$, the photon escapes; otherwise it is absorbed by a particle at a distance S along the direction θ from the point of emission. The absorbed energy is not placed in one state, rather, it is distributed over all states.

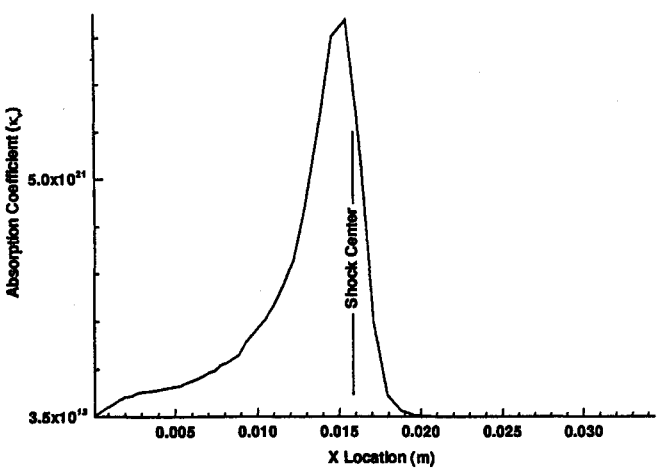

Fig. 1 Absorption coefficient for $N_2(2+)$ system.

Ionization Model

To simplify the calculations, Bird's ionization model,[15] in which each electron is associated with an ion and the two are marched as a pair, is employed. The more elaborate ambipolar diffusion model of Carlson and Hassan[16] adds a great deal of complexity to the calculations because it calculates an electric field as part of the solution.

Results and Discussion

The flow conditions are those representative of a 10 km/s standing normal shock wave in air at a pressure of 0.1 torr. Comparisons of theory and experiment involve DSMC calculations using two absorption models, continuum calculations of Sharma and Whiting,[10] and the experiments of Sharma et al.[9] All results computed with the present absorption model are designated present, whereas those of Ref. 6 are designated Taylor. The temperature profiles obtained from the DSMC code prior to including radiation modeling are shown in Fig. 2. The flow was from right to left with the wall located at $x = 0$ cm. The shock center, defined for discussion purposes as the location where the density reached a value six times that of the freestream, stood approximately 1.6 cm from the wall. As seen in the figure this region was characterized by a high degree of thermal nonequilibrium. Downstream of the shock, near-thermal equilibrium was established. While the collisionally limited vibrational mode did not quite equilibrate with the other three modes, it did reach a reasonable steady state.

The effect of incorporating the present radiation model upon the temperature profiles is shown in Fig. 3. As can be seen,

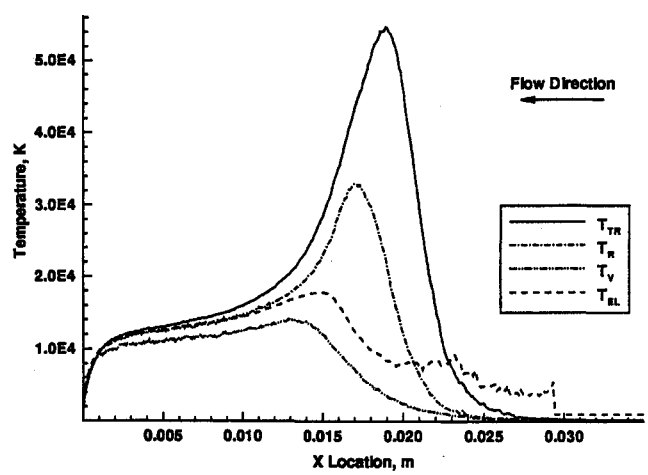

Fig. 2 Stagnation streamline temperature profiles without radiation.

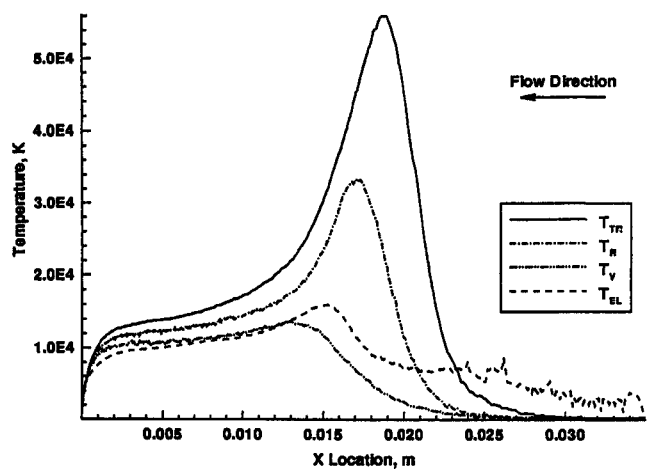

Fig. 3 Stagnation streamline temperature profiles with radiation.

radiation depleted energy from the electronic mode, disturbing the near equilibrium of Fig. 2; the other modes were not quite able to re-equilibrate with the electronic mode before reaching the wall. In spite of this, an approximate steady state was achieved and this region will be referred to as equilibrium. Similar behavior is indicated with the Taylor model.

Reference 7 reported that the equilibrium temperature after the shock, corresponding to radiative equilibrium, was 9650 ± 250 K. Reference 9 reaffirmed this measurement, indicating a T_{eq} of 9620 K. Although one particular equilibrium temperature is difficult to extract from the simulation temperature profiles, it was chosen as the temperature corresponding to the x location of the postshock inflection point in the density profile. At this location, $x = 0.4116$ cm, the temperatures and density reached their best steady state free of the effects of the wall. According to the previous definition the present model achieved an electronic temperature of 9930 K and the Taylor model reached 10075 K, both in reasonable agreement with the experimental results.

Figure 4 shows the global radiation profiles for both the present and Taylor models. As can be seen in Fig. 4a the absorption profile in the present model closely followed emission, indicating that absorption distances were typically small. The displacement of the emission and absorption curves is representative of the fact that many radiated photons, about 42%, escaped the flowfield without being absorbed. The figure also provides evidence of the precursor radiation, indicated by the nonzero absorption values in the inflow region. The peak nonequilibrium radiation occurred at 1.43 cm, slightly behind the shock center. The ratio of peak nonequilibrium to equilibrium radiation (corresponding to the equilibrium temperature as determined earlier) was 8.88, a value somewhat higher than the 4.5 reported in Ref. 9.

Figure 4b shows that the Taylor absorption model yielded dramatically different global radiation profiles than the present model. Emission and absorption are virtually coincident, suggesting a false state of radiative equilibrium in each supercell. Because the model underestimates the absorption coefficient, the distance over which absorption may take place [see Eq. (8)] is increased. As a result, only 27% of radiated photons escaped without being absorbed. Also, the ratio of peak nonequilibrium to equilibrium radiation was 7.98.

The greater amount of retained energy within the flow of the Taylor model meant higher ionization levels than the present model. In the Taylor model, the flow was 0.74% ionized, whereas in the present model it was 0.68% ionized. Both values are small, substantiating the weakly ionized assumptions made in calculations, but neither agrees with the 10 ± 2% ionization reported in the AVCO data.[7] The means of determining this value are not specified, however; presumably it was determined from a solution of the Saha equation.

Despite the disagreement between the two absorption models in the percent ionization and the global radiation profiles, both methods generated extremely similar atomic spectra. Because the earlier DSMC simulation[4] was compared with the results of the AVCO experiment, and Refs. 7 and 9 were in good agreement, the present comparisons will be limited to comparisons with both the experiment and the computation of Sharma et al.[9,10] Note that when making comparisons between the simulation results and experiment direct line-by-line comparisons cannot be made because of the groupings of electronic levels in the DSMC code. Furthermore, simulation results are only presented within the 3000–7000 Å wavelength range reported by Sharma et al., although the DSMC code included many transitions above and below this range (see Table 1). It

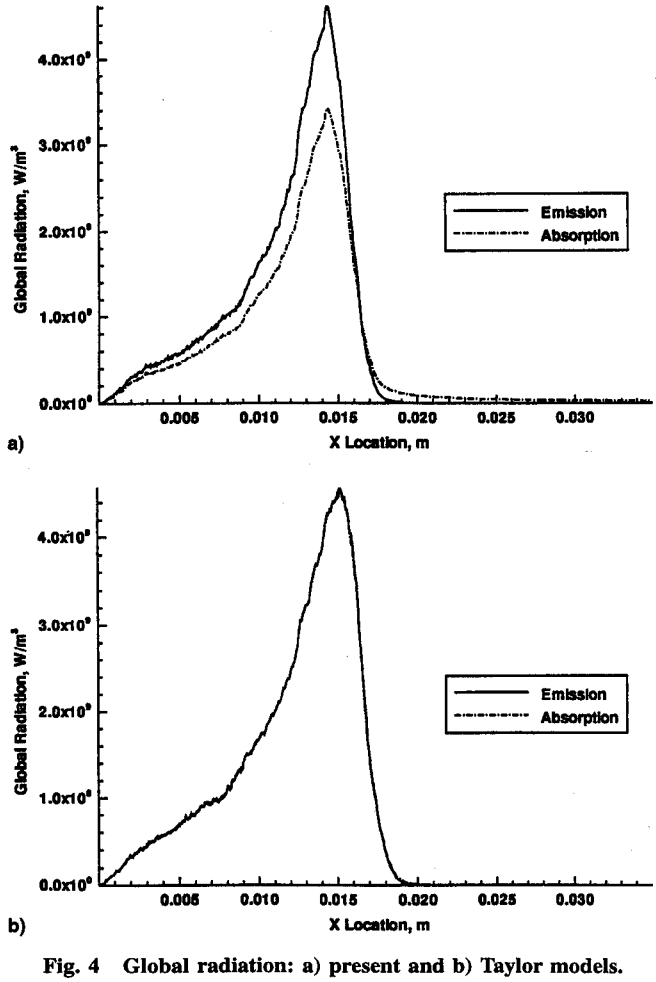

Fig. 4 Global radiation: a) present and b) Taylor models.

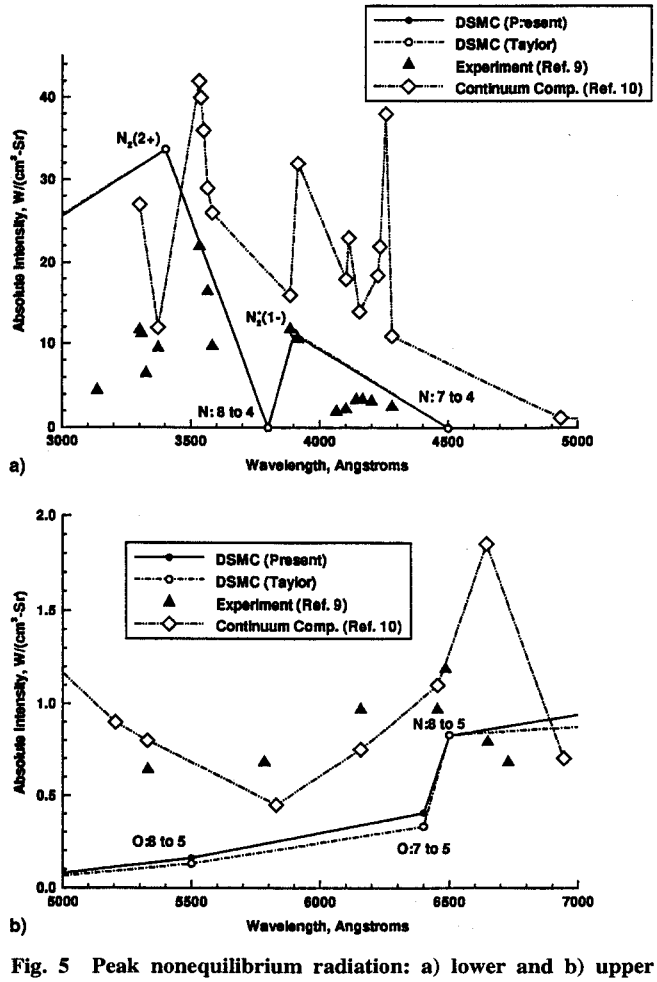

Fig. 5 Peak nonequilibrium radiation: a) lower and b) upper regions.

is in the lower wavelengths that the Taylor model displayed marginally higher intensities than the present model, thus accounting for the greater absorbed global energy in the Taylor model as shown in Fig. 4b. To clearly exhibit the various comparisons, the wavelength range is split into two regimes: the first covers the range 3000–5000 Å, whereas the second covers 5000–7000 Å.

Nonequilibrium Region

Figure 5a shows that the intensity of the $N_2^+(1-)$ system was well predicted by all computations, whereas that of the $N_2(2+)$ was overpredicted by DSMC. Moreover, Fig. 5b shows that intensities of the atomic lines were, in general, underpredicted. It is to be noted, however, that predictions were within a factor of 2–3. The atoms and their associated transitions are listed in the figures. As may be seen in the figure, the results of Ref. 10 are consistently higher for the higher wavelengths. Comparison of the calculated intensities of the $N_2^+(1-)$ system with those of Ref. 4 shows that inclusion of an absorption model is important for the conditions under consideration.

Equilibrium Region

Figure 6a shows that the intensities of both $N_2(2+)$ and $N_2^+(1-)$ are in good agreement with experiment, whereas Fig. 6b shows that intensities in the upper wavelengths were underpredicted by a factor as high as 4. In general, the intensities predicted by the simulation are higher than those of Ref. 10 below about 4000 Å and lower above 4000 Å.

As may be seen from the previous results, the two absorption models yield similar intensities (see Figs. 5 and 6). Examination of the equation of radiative transfer[17] suggests that a key parameter in determining the intensity is the optical thickness, i.e.,

$$\int_0^S \kappa_\upsilon \, ds \tag{12}$$

Although the two methods for selecting κ_υ^* are different, the absorption distance is chosen to satisfy Eq. (8), resulting in about the same optical thickness. Thus, as long as the calculated optical thickness is comparable, similar intensities will be calculated for a given set of boundary conditions.

Differences between DSMC and continuum[10] computations are to be expected. The continuum approach has many more levels, but DSMC calculations do not make use of two troublesome assumptions that are made in continuum calculations. These are the quasi-steady-state approximation and the need to assign one vibrational and one rotational temperature to all of the molecular species present. Both approaches, however, suffer from a lack of reliable rate data. As was shown in Ref. 4, relaxation numbers, which were estimated from available rate data, play a significant role in determining the various results.

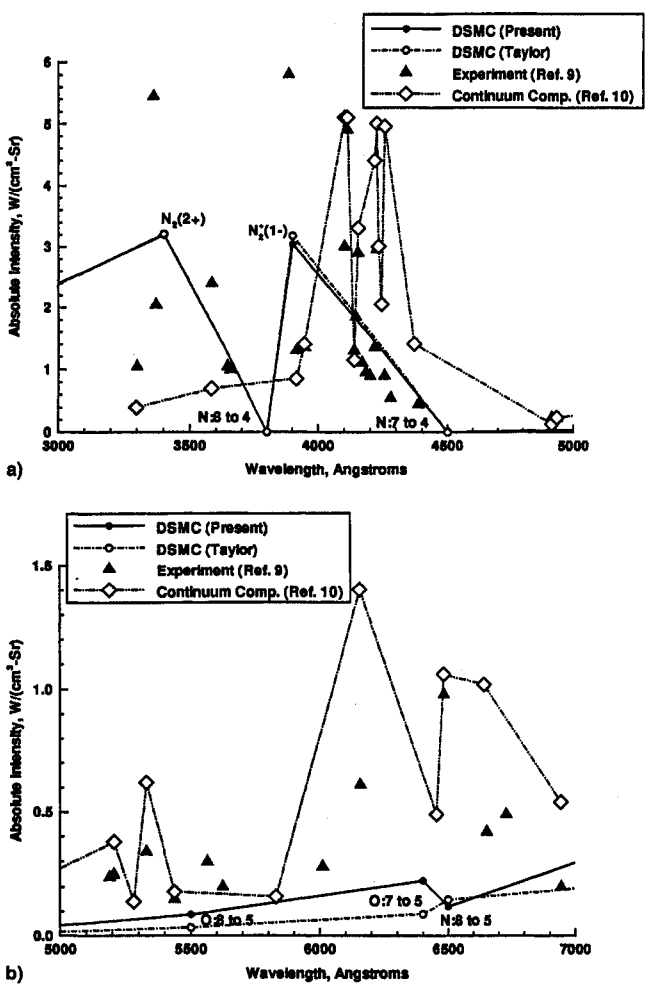

Fig. 6 Steady-state radiation: a) lower and b) upper regions.

Concluding Remarks

To more accurately simulate radiation at hypersonic speeds, a new absorption model has been implemented in a DSMC simulation of shock front radiation. Based on the agreement with measured intensities of the $N_2^+(1-)$ system, which eluded previous attempts, it is concluded that inclusion of appropriate absorption models is important in radiation calculations.

The two absorption models employed gave essentially identical intensities. This is because both models yielded nearly the same optical thicknesses. Thus, future applications may employ either model.

In spite of the fact that the model was limited to bound–bound radiative transitions and employed inadequate treatment of the electric field, present predictions suggest that DSMC methods are highly suited for radiation calculations at hypersonic speeds. Moreover, with improved computational capabilities in the future, more transitions and the effects of impurities can be accommodated.

Acknowledgments

Support for this work is provided by NASA's Cooperative Agreement NCCI-112 and the Mars Mission Research Center under NASA Grant NAGW-1331.

References

[1]Bird, G. A., *Molecular Gas Dynamics and the Direct Simulation of Gas Flows*, Clarendon, Oxford, England, UK, 1994.

[2]Bird, G. A., "Nonequilibrium Radiation During Re-Entry at 10 km/s," AIAA Paper 87-1543, June 1987.

[3]Moss, J. N., Bird, G. A., and Dogra, V. K., "Nonequilibrium Thermal Radiation for an Aeroassist Flight Experiment Vehicle," AIAA Paper 88-0081, Jan. 1988.

[4]Carlson, A. B., and Hassan, H. A., "Radiation Modeling with Direct Simulation Monte Carlo," *Journal of Thermophysics and Heat Transfer*, Vol. 6, No. 4, 1992, pp. 631–636.

[5]Taylor, J. C., Carlson, A. B., and Hassan, H. A., "Monte Carlo Simulation of Radiating Re-Entry Flows," *Journal of Thermophysics and Heat Transfer*, Vol. 8, No. 3, 1994, pp. 478–485.

[6]Taylor, J. C., Hassan, H. A., and Chambers, L. H., "A Radiation Absorption Model for the DSMC Method," *Rarefied Gas Dynamics 19*, edited by J. Harvey and G. Lord, Vol. 2, Oxford, England, UK, 1995, pp. 829–834.

[7]Allen, R. A., Rose, P. H., and Camm, J. C., "Nonequilibrium and Equilibrium Radiation at Super-Satellite Reentry Velocities," AVCO-Everett Research Labs, Research Rept. 156, Everett, MA, 1962.

[8]Park, C., "Nonequilibrium Air Radiation (NEQAIR) Program: Users Manual," NASA TM 86707, July 1985.

[9]Sharma, S. P., Gillespie, W. D., and Meyer, S. A., "Shock Front Radiation Measurements in Air," AIAA Paper 91-0573, Jan. 1991.

[10]Sharma, S. P., and Whiting, E. E., "Modeling of Nonequilibrium

Radiation Phenomena: An Assessment," AIAA Paper 94-0253, Jan. 1994.

[11]Hash, D. B., and Hassan, H. A., "Direct Simulation with Vibration-Dissociation Coupling," AIAA Paper 92-2875, July 1992.

[12]Borgnakke, C., and Larsen, P. S., "Statistical Collision Model for Monte Carlo Simulation of Polyatomic Gas Mixtures," *Journal of Computational Physics*, Vol. 18, No. 3, 1975, pp. 405–420.

[13]Modest, M. F., *Radiative Heat Transfer*, McGraw–Hill, New York, 1993, pp. 489, 490.

[14]Hartung, L. C., "Development of a Nonequilibrium Radiative Heating Prediction Method for Coupled Flowfield Solutions," *Journal of Thermophysics and Heat Transfer*, Vol. 6, No. 4, 1992, pp. 618–625.

[15]Bird, G. A., "Direct Simulation of Typical AOTV Entry Flows," AIAA Paper 86-1310, June 1986.

[16]Carlson, A. B., and Hassan, H. A., "Direct Simulation of Reentry Flows with Ionization," *Journal of Thermophysics and Heat Transfer*, Vol. 6, No. 3, 1992, pp. 400–404.

[17]Vincenti, W. G., and Kruger, C. H., Jr., *Introduction to Physical Gas Dynamics*, Krieger, Malabar, FL, 1965, pp. 462–464.